



Column-Integrated Aerosol Optical Properties during Summer and Autumn of 2012 in Xi'an, China

Xiaoli Su¹, Junji Cao^{1,2*}, Zhengqiang Li³, Meijing Lin⁴, Gehui Wang¹

¹ Key Laboratory of Aerosol Science & Technology, SKLLQG, Institute of Earth Environment, Chinese Academy of Sciences, Xi'an 710075, China

² Department of Environmental Science and Engineering, Xi'an Jiaotong University, Xi'an 710049, China

³ Institute of Remote Sensing and Digital Earth, Chinese Academy of Sciences, Beijing 100101, China

⁴ Zhongshan Bureau of Meteorology, Zhongshan 528400, China

ABSTRACT

Column-integrated aerosol optical properties were derived systematically from measurements made in Xi'an, which is located in Guanzhong Plain of central China with a ground-based CIMEL sun photometer from May to November 2012. Aerosol optical depths (AODs), Ångström exponents, water vapor contents, and aerosol optical and micro-physical properties, including aerosol volume size distribution, complex refractive indices and single scattering albedo (SSA), were determined. Daily variations in AODs at 440 nm (τ_{440}) generally followed those of the 24-hr PM_{2.5} mass concentrations, but there were differences in the relationships in summer and autumn. August showed the highest monthly τ_{440} (1.13) while the largest monthly Ångström exponent ($\alpha_{440-870} = 1.30$) and water vapor content ($C_w = 4.28$) both occurred in July. Monthly averages of the aerosol size distributions showed the dominance of coarse mode aerosols, except in July and August, when the contribution of the accumulation and coarse modes were fairly comparable. Monthly changes in the complex refractive index (including both real and imaginary parts) and SSA were also studied, including their wavelength dependences; these analyses implied changes in the abundances of the aerosol types. Finally, an episode involving urban and dust aerosols was analyzed using sun photometer aerosol retrievals; MODIS images captured by Aqua satellite and average wind vectors from the NCEP operational global analyses were also considered in the case study.

Keywords: Aerosol optical depth; Ångström exponent; Water vapor content; Aerosol optical properties; Sun photometer.

INTRODUCTION

Atmospheric aerosols are important in the global climate system due to the key roles they play in the atmospheric radiation budget, cloud formation and hydrological cycle. The effects of aerosols on climate are normally quantified in terms of aerosol radiative forcing, which depends strongly on the particles optical properties (OPs). Thus, comprehensive knowledge of aerosol OPs is critical not only for current assessments but also for predictions of future changes in regional and global climate. The high spatial and temporal variability of the number, size and composition of the aerosols makes their effects one of the greatest sources of uncertainty in climate modeling and prediction (Formenti *et al.*, 2011; Mahowald *et al.*, 2011). This is despite the fact that much attention has been paid to these issues, and

significant progress has indeed been made in the past several decades (Holben *et al.*, 2001; Kaufman *et al.*, 2002; Smirnov *et al.*, 2002a; Lohmann and Feichter, 2005; Kambezidis and Kaskaoutisa, 2008; Quaas *et al.*, 2008; Li *et al.*, 2011; Yoon *et al.*, 2012).

China has experienced rapid industrial growth and urbanization since the mid-1970s, and as an unfortunate result, much of the country suffers from aerosol pollution (Qiu and Yan, 2000; Luo *et al.*, 2001; Xia *et al.*, 2007b; de Meij *et al.*, 2012; Yoon *et al.*, 2012). The high aerosol loadings in China result from a complex mixture of particles that originate from a variety of anthropogenic sources, especially coal combustion, motor vehicle emissions, and biomass burning, as well as dust storms (Li, 2004; Jin and Shepherd, 2005; Zhao and Li, 2007). The complex sources and formation mechanisms of aerosols over China make it difficult to adequately characterize the aerosol physical and radiative properties over such a vast territory (Roger *et al.*, 2009). Even so, numerous studies have been conducted in recent years to investigate the aerosol OPs over China, (Li *et al.*, 2003; Garland *et al.*, 2008; Xie and Xia, 2008; He *et al.*, 2009; Fan *et al.*, 2010; Su *et al.*, 2010; Ma *et al.*,

* Corresponding author.

Tel.: 86-029-88326488; Fax: 86-029-88320456
E-mail address: cao@loess.llqg.ac.cn

2011; Chen *et al.*, 2012; Wu *et al.*, 2012; Xu *et al.*, 2012; Yan *et al.*, 2013).

The aerosol optical depth (AOD) over China has shown an increasing trend, from 0.38 in 1960 to 0.47 in 1990; these findings were based on the measurements from 46 solar radiation stations (Luo *et al.*, 2001). Yoon *et al.* (2011) detected an increasing trend in AOD at both 443 and 555 nm over Pearl River Delta of South China from 1997 to 2008 with magnitudes of 0.00761 and 0.00635 yr⁻¹, respectively. In addition to the analyses of long-term trends in AOD, studies have related the spatial and temporal patterns of aerosol OPs to the various aerosol types.

Along these lines, the optical properties of urban aerosols were analyzed using data from CE-318 sun photometers deployed at Shanghai (Song and Lu, 2006; He *et al.*, 2012), Hangzhou and other sites in the Chinese Yangtze Delta Region (Pan *et al.*, 2010; Chen *et al.*, 2012). Xia *et al.* (2004) and Che *et al.* (2009a) studied the OPs and seasonal variability of mineral aerosol at Dunhuang and Yulin, which are in the semi-arid regions of Northwest China, and Che *et al.* (2013) studied the variations in aerosol optical properties over the Taklimakan Desert. Aerosol OPs also have been retrieved from sun photometer measurements at several regional background stations, including Longfengshan, Lin'an, Shangdianzi and Waliguan (Che *et al.*, 2009b; Wang *et al.*, 2010; Che *et al.*, 2011). Che *et al.* (2009b) have attempted to link aerosol optical properties at the first of these three sites to their chemical composition. Moreover, Cong *et al.* (2009) analyzed aerosol optical properties at Nam Co, a remote site in the central Tibetan Plateau; that study filled a gap in the aerosol data for the large high-elevation area.

Based on the analyses of aerosol optical properties, studies on the radiative effects of aerosols have also been carried out at Taihu, a site surrounded by several large cities in the Yangtze delta region, southern China (Xia *et al.*, 2007a); at Beijing, located at the northern tip of the North China Plain (Xia *et al.*, 2007b); at Xianghe in Northern China (Li *et al.*, 2007); and Lanzhou in Northwest China (Liu *et al.*, 2011). Much of the previous research has focused on the North

China Plain, especially at Beijing; the coast of southeastern China (e.g., the Pearl River Delta region); and some of the arid and semi-arid lands in northwest China. In comparison, very few studies have investigated aerosol optical properties over the central China.

The main objective of this study is to characterize the aerosol optical properties at Xi'an, which lies in the Guanzhong Plain of central China. First, time-series of daily AOD at 440 nm derived from measurements taken with a ground-based sun photometer were analyzed and compared with 24-hr mean PM_{2.5} concentrations; these measurements were made from the middle May to the beginning of November 2012. For the investigations of aerosol optical properties, we compiled the statistics for monthly AOD at 440 nm (τ_{440}), Ångström exponent ($\alpha_{440-870}$) and column water vapor content (C_w , in cm). Aerosol microphysical properties were determined to further characterize aerosol concentrations in Xi'an and to relate the loadings to the optical data; these measurements included size distribution, refractive index, and single scattering albedo (SSA), including wavelength dependence ($\omega_0(\lambda)$). Finally, we analyzed a case study based on the measurements obtained with a Sun photometer; this involved combining the photometer data with MODIS observations and data from the NCEP FNL (Final) Operational Model Global Tropospheric Analyses dataset.

MEASUREMENTS AND METHODOLOGY

Site Description

The sun photometer used in this research was installed on the roof of the main building of the Institute of Earth Environment, Chinese Academy of Sciences (IEECAS: 34.22°N, 108.87°E; elevation = 389 m). Fig. 1 shows the location of the IEECAS site (marked by the blue dot) and the topography surrounding Xi'an, which is situated in the Guanzhong Plain. The colour bar in Fig. 1(b) is a key, showing the elevation in meters. Also known as the Central Shannxi Plain, the Guanzhong Plain is defined here as the area in China from 30°N to 40°N latitude and 105°E to 115°E

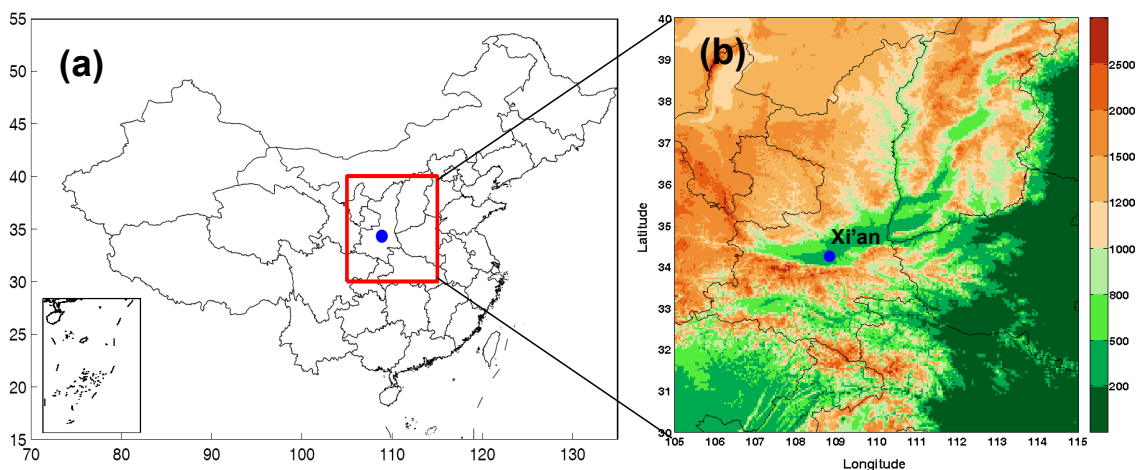


Fig. 1. Location of Sun photometer and the geography surrounding Xi'an, China. The color bar shows the altitude above sea level (in meters).

longitude; this is a topographic basin surrounded by Qinling Mountains to the south and the Loess Plateau to the north.

As the largest city in the central-northwestern China, Xi'an has achieved rapid economic growth and a flourishing tourist industry; this has been stimulated by the national policy for the Great Development of China's West. Unfortunately, the region suffers from severe air pollution due to the emissions of aerosol particles from industries and other human activities. Therefore, Xi'an can be considered a typical city in north China with significant air pollution problems, and it is well suited for investigating the contributions from both natural and anthropogenic aerosol sources (Zhang *et al.*, 2002). During the past several decades, numerous studies have characterized the aerosol chemical components in this city, such as organic carbon (OC), elemental carbon (EC) and water-soluble ions (e.g., sulphate, nitrate, and ammoniate); several of the studies investigated aerosols in different size ranges (Cao *et al.*, 2005, 2009; Shen *et al.*, 2009, 2010; Cao *et al.*, 2011; Shen *et al.*, 2011). Furthermore, source apportionments of size-resolved aerosols and their impacts on aerosol optical properties (such as aerosol horizontal extinction coefficient and visibility) have also been conducted by Che *et al.* (2006) and Cao *et al.* (2012). Nonetheless, aerosol optical properties in Xi'an have received little attention in the past, and therefore, it is important to improve our understanding of the aerosol over this region.

Data Collection and Methodology

Observations of columnar aerosol optical properties in this study were conducted during the daytime with the use of a Cimel CE318-NE type sun-sky radiometer (*Cimel Electronique, Paris, France*). This instrument was installed in the middle of May 2012, and it has been running continuously since then. The radiometer makes direct solar measurements with a 1.2° full field of view in nine bands (340, 380, 440, 500, 675, 870, 940, 1020 and 1640 nm nominal wavelength) about every fifteen minutes in accordance with scheduled procedures. Solar extinction measurements at 940 nm, were used to obtain the column water vapor content while direct sun measurements of AOD at 440 and 870 nm (Holben *et al.*, 1998; Dubovik *et al.*, 2000) were used to derive the SSA (Holben *et al.*, 1998, 2001; Eck *et al.*, 2005). In addition to direct solar radiation measurements, the sun photometer also performs sky radiance scans at 440, 675, 870, and 1020 nm. Aerosol microphysical properties, including size distribution, refractive index, and SSA, can be retrieved from the sky radiance measurements in conjunction with direct solar measurements of AOD at 440, 675, 870, and 1020 nm (Dubovik *et al.*, 2000; Dubovik and King, 2000; Dubovik *et al.*, 2006; Li *et al.*, 2009).

In this study, the comprehensive aerosol retrieval code developed by Dubovik *et al.* (2000, 2006) is utilized to retrieve aerosol optical properties. To ensure the quality of aerosol inversions from the sun photometer data, cloud screening and a quality control algorithm developed by Smirnov *et al.* (2000) were employed in conjunction with

the retrievals of the aerosol optical properties. The instrument calibration (sun and sky measurement calibration on 16 March 2012) and derivation of AOD are discussed in detail in Holben *et al.* (1998) and Li *et al.* (2008). The total uncertainty in aerosol optical depth retrieved from sun photometer measurements using the above algorithms is about 0.01–0.02 (Eck *et al.*, 1999). To summarize: the aerosol optical properties discussed in this paper were τ_{440} , $\alpha_{440-870}$, n , $\omega_0(\lambda)$ (at wavelengths, λ , of 440, 670, 875 and 1020 nm), and volume size distribution (from 0.05 to 15 μm).

Besides the columnar aerosol optical properties obtained with the sun photometer, mass concentrations of $\text{PM}_{2.5}$ (particles < 2.5 μm in aerodynamic diameter) were measured with an E-BAM-9800 particulate monitor (*Met One Instruments, Inc.*). These $\text{PM}_{2.5}$ loadings were used for comparisons with aerosol optical properties. Additionally, satellite observations and meteorological data were also included in a case study; these include Aqua MODIS (Moderate Resolution Imaging Spectroradiometer) true color images and wind vectors from the NCEP FNL Operational Model Global Tropospheric Analyses (GRIB 2, on 1.0×1.0 degree grids, <http://rda.ucar.edu>).

RESULTS AND DISCUSSION

Evolution of Daily AOD at 440 nm and 24-hr Mean $\text{PM}_{2.5}$ Concentrations

Daily AOD averages were calculated from all measurements for each day when three or more measurements were available: the daily averages were then used to compute the corresponding monthly averages. Due to cloud contamination and instrument problems, several interruptions appeared in the time-series of the daily τ_{440} in Fig. 2, which is presented along with the 24-hr average $\text{PM}_{2.5}$ concentrations (in $\mu\text{g}/\text{m}^3$). The error bars in Fig. 2 implied the diurnal variation of AOD for the given day. As shown in Fig. 2, daily variations in AOD were generally synchronous with $\text{PM}_{2.5}$ loadings, but the ranges of the variables and strengths of the relationships varied with season. That is, the daily AOD co-varied with the 24-hr average $\text{PM}_{2.5}$, but the correlation was stronger during the summer months (the correlation coefficients, r , were $r = 0.69$ for the summer months and $r = 0.50$ and autumn, respectively). Additionally, the daily τ_{440} was comparatively more variable than $\text{PM}_{2.5}$ in summer, especially in July and August, and less so in autumn. Consequently, a marked difference in the seasonality of τ_{440} and $\text{PM}_{2.5}$ can be seen in Fig. 2.

The AOD showed its maximum in summer ($\tau_{440} = 3.55$ on Jul. 18) while the maximum $\text{PM}_{2.5}$ loading occurred in autumn on Oct. 29, with a value of 274.69 $\mu\text{g}/\text{m}^3$. The average AODs in the summer (JJA) and autumn (SON) months were 1.09 ± 0.77 (mean \pm SD) and 0.65 ± 0.39 respectively. By way of contrast, the mean $\text{PM}_{2.5}$ values in summer and autumn were 60.01 ± 27.74 $\mu\text{g}/\text{m}^3$ and 94.39 ± 50.09 $\mu\text{g}/\text{m}^3$, respectively. The standard deviations, which reflect the day-to-day variability in AOD and $\text{PM}_{2.5}$, confirmed the change in aerosol populations for the two seasons noted above (Table 1).

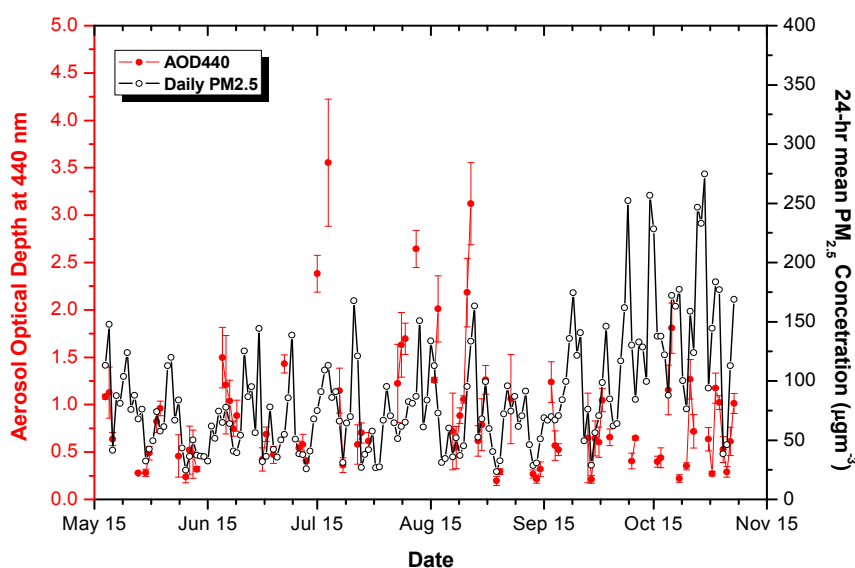


Fig. 2. Time-series of daily AOD at 440 nm and 24-hour average $PM_{2.5}$ concentrations over Xi'an from May to November of 2012.

Table 1. Summary of the measurements obtained with a sun photometer deployed at the IEECAS site (Latitude: 34.22°N, Longitude: 108.87°E, elevation: 389m) 18 May to 6 November 2012, including aerosol optical depth (τ_{440}), Ångström exponent ($\alpha_{440-870}$), water vapor content (C_w) and their associated standard deviations σ_τ , σ_α and σ_w . The number of measurements (N_{meas}) and days (N_{day}) in the corresponding months used for statistical calculations are also presented.

Month	τ_{440}	σ_τ	$\alpha_{440-870}$	σ_α	C_w (cm)	σ_w	N_{meas}	N_{day}
May	0.62	0.38	0.97	0.25	2.23	0.39	127	7
Jun	0.75	0.39	1.19	0.19	2.91	0.68	270	16
Jul	0.75	0.62	1.30	0.18	4.28	0.68	204	20
Aug	1.13	0.69	1.24	0.19	3.73	1.01	205	21
Sep	0.46	0.31	1.26	0.25	1.82	0.65	326	16
Oct	0.60	0.42	0.96	0.28	1.28	0.62	343	18
Nov	0.59	0.30	0.78	0.40	0.66	0.38	168	6

To understand the causes of these differences in the seasonal variability in columnar AOD and $PM_{2.5}$ mass concentrations, it is instructive to first consider their definitions. As the integral of the extinction coefficient from the surface (ground level) to the top of atmosphere, columnar AOD is a measure of the total aerosol loading in a vertical atmospheric column of unit cross section. In contrast, the $PM_{2.5}$ loading measures the mass of dry particles $< 2.5 \mu m$ aerodynamic diameter in a volume of air, which in our study was collected near the surface. Therefore, the observed differences can be attributed not only to the seasonal variability in the vertical structure of aerosol layers and the aerosol chemical composition and size distribution, but also to the changes in meteorological conditions (such as relative humidity) that affect the aerosol column. Despite the numerous factors that can potentially confound the relationship between AOD and surface-level $PM_{2.5}$, the AOD retrievals implied the possibility of estimating $PM_{2.5}$ from ground-based measurements obtained with sun-sky radiometers.

Summary Statistics for Aerosol Optical Depth, Ångström Exponent and Water Vapor Content

Monthly statistics for τ_{440} , $\alpha_{440-870}$, and C_w , which were obtained from direct solar measurements made with the sun photometer, are presented as box-and-whiskers plots in Figs. 3(a), 3(d) and 3(g), along with their probability distributions for summer and autumn (Figs. 3(b), 3(c), 3(e), 3(f), 3(h) and 3(i)). In the box plots, the ends of each box represent the 25th and 75th percentiles of the distributions, the ends of the whiskers represent the standard deviations, and the lines across the box are medians. The mean, maximum and minimum of the distributions are represented by the open squares, filled circles and open circles, respectively. A summary of the results from the statistical analyses is given in Table 1, including monthly average τ_{440} , $\alpha_{440-870}$, and C_w , as well as their associated standard deviations. The numbers of measurements and days in the months used for statistical calculations are included in the table. Note that there were fewer than 10 days with available daily measurements in May and November. Therefore, the data summaries may not fully represent the characteristics of aerosols for those two months. Even so, the data for all available monthly averages are discussed below.

The monthly trends in τ_{440} , $\alpha_{440-870}$, and C_w are shown in Figs. 3(a), 3(d) and 3(g). The monthly maxima for all three

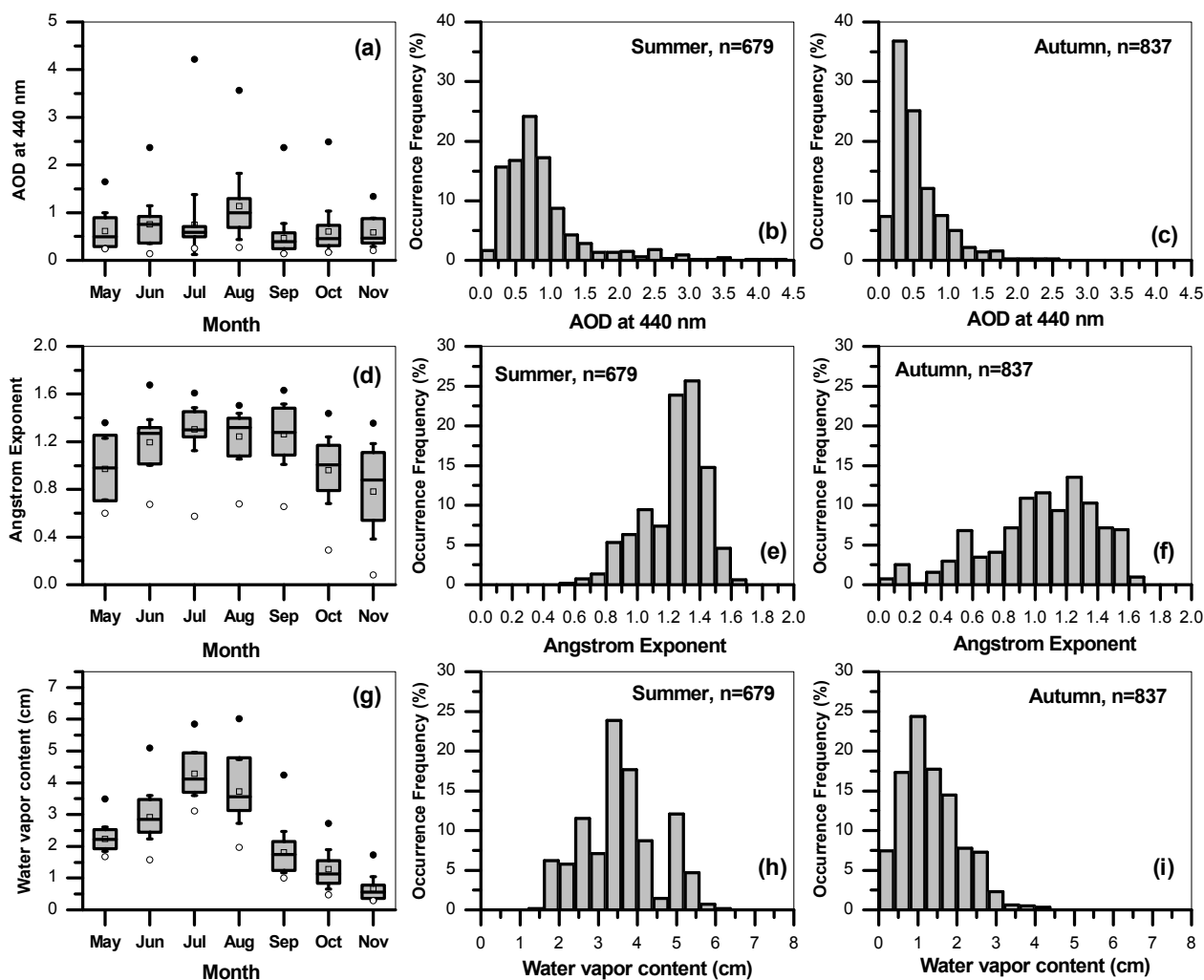


Fig. 3. Box plots of (a) monthly aerosol optical depth, (d) Ångström exponent and (g) water vapor content during the study period and their associated frequencies of occurrence in summer (June–July–August) and autumn (September–October–November) of 2012.

of these parameters occurred in the summer months. That is, the highest monthly AOD appeared in August, with the value of 1.13 ± 0.69 , while $\alpha_{440-870}$, and C_w showed their maxima in July, with the values of 1.30 ± 0.18 and 4.28 ± 0.68 cm. The more abundant water vapor and higher temperatures in summer may have promoted the conversion of gaseous species to particulates, resulting in more hygroscopic aerosols and thus higher AODs. With reference to the minima of aerosol properties, AOD showed its lowest value in September while in contrast both $\alpha_{440-870}$ and C_w exhibited their minima in November. The low $\alpha_{440-870}$ in May and November (0.97 and 0.78) may reflect the influence of coarse-mode dust in spring and autumn. Generally, the variability in the monthly Ångström exponent, which ranged from 0.78 to 1.30, implies a mixture of fine- and coarse-mode aerosol particles in Xi'an.

The probability distributions of the daily average τ_{440} , $\alpha_{440-870}$, and C_w in summer and autumn are shown in Figs. 3(b), (c), (e), (f), (h) and (i). It is evident that the atmosphere was at times more turbid in summer than in autumn and also overall more variable because the distribution of τ_{440}

was wider in summer (compare Figs. 3(b) and 3(c)). Almost 10% of daily average τ_{440} were > 1.50 in summer while in contrast, about 70% of daily τ_{440} were < 0.50 in autumn. Conversely, the daily Ångström exponent distribution was much narrower in summer than in autumn (Figs. 3(e) and 3(f)). All of the daily values of $\alpha_{440-870}$ were > 0.5 in summer, whereas $\sim 8\%$ of the daily $\alpha_{440-870}$ were < 0.5 in autumn. The seasonally averaged values for $\alpha_{440-870}$ in summer and autumn were 1.24 ± 0.19 and 1.04 ± 0.35 , respectively. As for the water vapor content (C_w), the width of its distribution in summer was comparable to that in autumn, but the ranges were noticeably different. That is, the C_w values in summer were clearly higher than those in autumn; and this can be seen in their seasonal averages (3.57 ± 0.98 cm in summer versus 1.37 ± 0.73 cm in autumn).

Fig. 4 presents the scatter plots for $\alpha_{440-870}$ and C_w against τ_{440} in summer and autumn. The numbers of measurements included in this analysis were 679 and 837 for summer and autumn, respectively. As shown in Fig. 4(a), the dependencies of $\alpha_{440-870}$ on τ_{440} in the two seasons were slightly different. In summer, the majority of $\alpha_{440-870}$ for $\tau_{440} > 0.5$ ranged

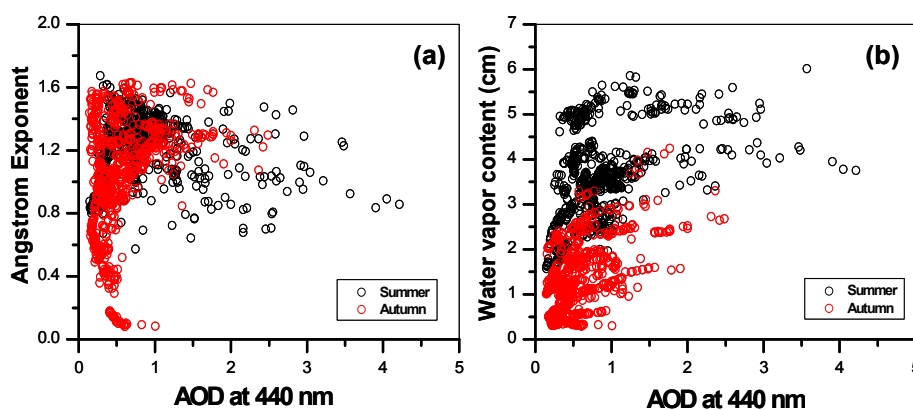


Fig. 4. Scatter plots of daily average Ångström exponent ($\alpha_{440-870}$) and water vapor content (C_w in cm) versus daily AOD at 440 nm (τ_{440}) in summer and autumn of 2012.

from 0.6 to 1.7, and this implies a mixed contribution of both fine-mode and coarse-mode particles to the total aerosol loading. In autumn, on the other hand, a relatively large spread in $\alpha_{440-870}$, which varied from 0 to 1.7 for low values of τ_{440} (that is, < 0.5), was observed. Large spreads in $\alpha_{440-870}$ at low to moderate τ_{440} have also been observed in some dust source regions (Smirnov *et al.*, 2002b, c; Xia *et al.*, 2004). Accordingly, we conclude that aerosol loads in Xi'an were greatly influenced by the coarse-mode fraction, especially in autumn.

Additionally, in both summer and autumn, the maximum $\alpha_{440-870}$ showed a weak decreasing trend with increasing τ_{440} ; indeed, when $\tau_{440} > 3.0$, all the $\alpha_{440-870}$ values were less than 1.4. Such a trend can be attributed to two factors. The first is the increased radius of the fine-mode particles when particle coagulation and hygroscopic growth cause an increase in τ_{440} . The decreasing trend in the maximum $\alpha_{440-870}$ with increasing τ_{440} in summer shown in Fig. 4(a) was mainly caused by this factor. The second factor is the increased contribution of coarse dust aerosols, which led to a decrease in $\alpha_{440-870}$ during autumn (Fig. 4(a) (Fan *et al.*, 2006).

As shown in Fig. 4(b), the daily average τ_{440} was positively correlated with C_w in both summer and autumn, with $r = 0.43$ and 0.51 , respectively. When τ_{440} ranged from 0 to 2.5, C_w varied from 1.5 to 6.0 in summer, but it was distributed over a lower range of 0 to 4.0 in autumn. Moreover, the minimum in C_w showed a clear increasing trend in summer when τ_{440} increased from 0.0 to 4.0. This may be related to the hygroscopic growth of aerosols promoted by the increased relative humidity or the coupling of water vapor and aerosol loadings from different source regions (Eck *et al.*, 2001; Fan *et al.*, 2006).

Monthly Variability of Aerosol Size Distribution, Spectral Single Scattering Albedo and Complex Refractive Index

The aerosol volume size distribution $dV(r)/d\ln r$ ($\mu\text{m}^3/\mu\text{m}^2$), SSA, and complex refractive index (RI, written as $n(\lambda) - k(\lambda)i$) were retrieved from spectral solar and sky radiance measurements using the algorithm of Dubovik *et al.* (2006). For these calculations, the retrievals of aerosol volume size distribution were performed in 22 logarithmically equidistant

bins in the range of sizes $0.05 \mu\text{m} \leq r \leq 15 \mu\text{m}$. The real $n(\lambda)$ ($1.33 \leq n(\lambda) \leq 1.7$) and imaginary $k(\lambda)$ parts of the complex refractive index ($0.0005 \leq k(\lambda) \leq 0.5$) were derived for the wavelengths of 440, 675, 870 and 1020 nm, as well as $\omega_0(\lambda)$. In the following section, we first consider the monthly variability in aerosol volume size distributions and then investigate the monthly-average spectral variations in the SSA and both the real and imaginary parts of the complex refractive index.

The aerosol volume size distribution $dV(r)/d\ln r$ ($\mu\text{m}^3/\mu\text{m}^2$) generally exhibited a bimodal structure, and it could be characterized by the sum of two log-normal distributions as follows:

$$\frac{dV(\lambda)}{d \ln r} = \sum_{i=1}^2 \frac{C_{V,i}}{\sqrt{2\pi}\sigma_i} \exp\left[-\frac{(\ln r - \ln r_{V,i})^2}{2\sigma_i^2}\right] \quad (1)$$

where $C_{V,i}$ is the volume concentration, $r_{V,i}$ is the volume median radius, and σ_i is the geometric standard deviation for mode i . The monthly averages of the aerosol volume size distribution retrievals from May to November of 2012 are presented in Fig. 5. The error bars, denoting the standard deviation, described the daily variation in aerosol size distribution for the given month. A consistent feature of the size distributions is the dominance of coarse-mode particles for most months, except July and August, when the contribution of accumulation and coarse modes were more comparable. Furthermore, in those two months, the contribution of the accumulation mode appeared to be higher than that in other studied months, but the fractions contributed by coarse mode were much lower.

The monthly variability in aerosol volume size distributions can be explained in two ways. First, Xi'an suffers from high particulate loadings, not only as a result of anthropogenic activities but also because large quantities of natural mineral dust are transported from remote deserts and the surrounding loess plateau. In addition, the so-called urban fugitive dusts (for example, construction dusts) can also increase the volume contribution of the coarse mode fraction. On the other hand, precipitation significantly increases in July and August due to effects of the East Asian Monsoon. Since

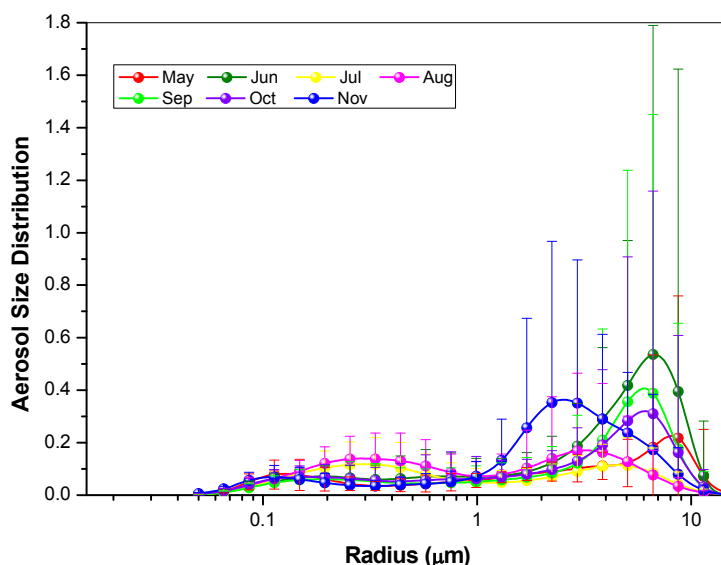


Fig. 5. Monthly average of aerosol size distribution retrievals from May to November of 2012 in Xi'an.

removal by wet deposition is generally considered to be greater for larger particles than for fine ones, the higher precipitation in July and August may suppress the production of dust. Moreover, the combination of high temperatures, high relative humidities, and low wind speeds in July and August favor particle growth and new particle formation (Yue *et al.*, 2009), and these factors probably contributed to the increased importance of fine mode aerosols in late summer.

The SSA is one of the key determinants of the radiative effects of the atmospheric aerosol. Defined as the ratio of scattering efficiency of the aerosols to their total extinction efficiency, it provides important information regarding scattering and absorption properties. The uncertainties for the SSAs in our study were estimated to be about 0.03 (Dubovik *et al.*, 2000). Monthly variations in $\omega_0(\lambda)$ are presented in Fig. 6(a). Generally, the monthly SSA averages in summer were higher than those in autumn. The highest monthly $\omega_0(440)$ occurred in August, with a value of 0.97 ± 0.02 , and the lowest monthly average $\omega_0(440)$ (0.85 ± 0.04) occurred in November.

The wavelength dependence of the monthly SSAs, which aids in identifying the sources for the aerosol, is presented in Fig. 6(a). Theoretically, SSA should increase rapidly with wavelength during dust events but decrease during periods of increased urban aerosol pollution (Dubovik *et al.*, 2002; Bergstrom *et al.*, 2007; Alam *et al.*, 2012). The SSA in November of 2012 showed a clear increasing trend with wavelength (Fig. 6(a)); this reflects the dominance of dust particles over anthropogenic aerosols in the atmosphere during the six days of this month for which data are available. The low SSA in this month can be explained by a combination of dust aerosols with absorbing anthropogenic aerosols. Along with $\omega_0(\lambda)$, monthly averages of both the real $n(\lambda)$ and imaginary $k(\lambda)$ parts of complex refractive index are presented in Figs. 6(b) and 6(c), respectively. The two parts of refractive index indicate the scattering and absorbing efficiencies of aerosol, and therefore, they are

helpful in identifying highly scattering or absorbing aerosols. As shown in Fig. 6(b), monthly $n(\lambda)$ values were slightly higher at longer wavelengths than shorter ones due to the increased absorption by coarse-mode aerosols in the near infrared band (Cheng *et al.*, 2006a, b). Monthly $n(\lambda)$ varied from a low of 1.46 ± 0.07 in August to a high of 1.58 ± 0.08 in June; although the two are both summer months, June and August showed markedly different values for $n(\lambda)$. This is likely related to the different volume size distributions in these two months; that is, a domination of the coarse mode over the accumulation mode in June compared with more similar contributions of the two modes in August.

The wavelength dependence of the imaginary component of the complex refractive index, $k(\lambda)$, is shown in Fig. 6(c). In general, $k(\lambda)$ varied inversely with wavelength, a trend opposite to that shown by the SSA. The monthly-averaged $k(\lambda)$ ranged from 0.005 at 1020 nm to 0.007 at 440 nm, and $k(\lambda)$ also varied from month-to-month. Unlike SSA, $k(\lambda)$ exhibited its maximum at 440 nm in November (0.018 ± 0.010) and its minimum in August (0.003 ± 0.003). In general, the values for $k(\lambda)$ were higher in autumn than in summer, and this can be attributed to the influence of dust aerosols and enhanced levels of anthropogenic absorbing particles, most likely those from straw burning or residential heating using coal and wood.

Columnar Aerosol Optical Properties during an Episode of Aerosol Pollution

In order to evaluate the capability of sun photometer in air pollution monitoring, we investigated an episode involving urban and dust aerosols, which occurred from 2 to 5 November 2012. The MODIS RGB images over Xi'an captured by the Aqua satellite during these days and associated wind vectors from the NCEP FNL Operational Model were used to supplement our ground-based measurements. The location of Xi'an is marked using red circles in the MODIS RGB images from 2 to 5 November in Figs. 7(a) to 7(d) and as black triangles the wind fields

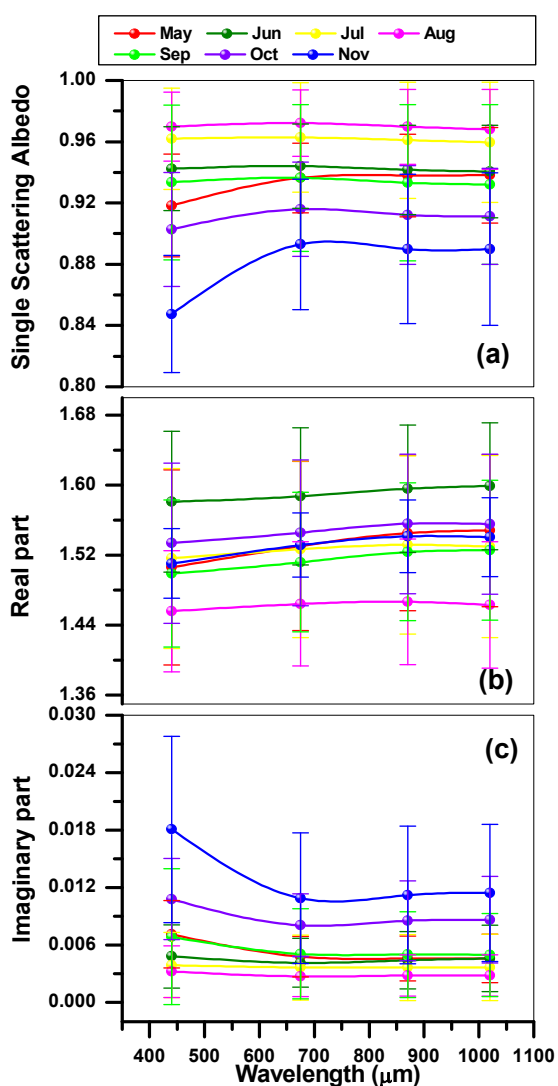


Fig. 6. Monthly variability of spectral SSA (a) and complex refractive index (including real part (b) and imaginary part (c)) from May to November of 2012 over Xi'an, where the standard deviation are also presented with error bars.

shown in Figs. 7(e) to 7(h), respectively. The day-to-day and diurnal variations in τ_{440} and $\alpha_{440-870}$ are evaluated in the following section. The corresponding standard deviations are also presented, although some of them are too low to be visible in Fig. 7.

The hourly averages of both τ_{440} and $\alpha_{440-870}$ were high and showed little diurnal variability on 2 November (1.02 ± 0.06 and 1.31 ± 0.04 , respectively; Fig. 7). The high values for τ_{440} and $\alpha_{440-870}$ implied urban aerosol pollution dominated by fine anthropogenic particles. The accumulation of local urban aerosols was also facilitated by the weak winds on this day (Fig. 7(e)). On the following day, τ_{440} showed a clear decreasing trend from the high value of 0.92 at 11:00 (local time) to 0.41 at ~16:00. The $\alpha_{440-870}$ values decreased sharply from the high values on 2 November to nearly zero on the next day, indicating that aerosol loadings on 3 November were mainly dominated by large dust particles.

The decreasing trend in τ_{440} may have been caused by the passage of a desert dust event, which was brought about by strong northwesterly winds (Fig. 7(f)) – the MODIS RGB image in Fig. 7(b) also recorded this dust case. The daily averages for τ_{440} and $\alpha_{440-870}$ on 3 November were 0.53 ± 0.18 and 0.13 ± 0.03 , respectively.

November 4 was a clear day, and this is evidenced by low values of τ_{440} , which ranged from 0.21 at 16:00 to 0.38 at 9:00. Hourly measurements of τ_{440} showed a slight decreasing trend, with two peaks at 9:00 and 14:00, which is when the working hours began. In contrast to τ_{440} , $\alpha_{440-870}$ exhibited an increase compared with the previous day. This probably is related to the eastward transportation of dust aerosols, which were carried away by strong winds (Fig. 7(g)). On the morning of 5 November, the accumulation of aerosol pollution was implied by a sustained increase of τ_{440} ; this continued until 14:00. $\alpha_{440-870}$ also showed an increase before 14:00, and this can be explained by an increasing contribution of anthropogenic particles. The weak winds shown in Fig. 7(h) were also favorable for the build-up of the pollution aerosol. The abrupt decrease in both τ_{440} and $\alpha_{440-870}$ after 14:00 remains to be explained and will require further analyses.

CONCLUSIONS

Column-integrated aerosol optical properties (τ_{440} , $\alpha_{440-870}$, and C_w) at Xi'an were evaluated based on measurements made from May to November 2012 with a ground-based CIMEL sun photometer installed on the roof of the main building of the IEECAS. Daily variations in τ_{440} generally followed those of the $PM_{2.5}$ mass concentrations, but there were differences in the relationships in summer and autumn. We also discussed the changes in the monthly means calculated from quality-assured daily measurements of τ_{440} , $\alpha_{440-870}$, and C_w . The highest monthly τ_{440} occurred in August, with the value of 1.13, while the largest monthly $\alpha_{440-870}$ (1.30) and C_w (4.28) appeared in July. Based on analyses of the monthly variability in volume size distributions, we found that the coarse mode aerosols dominated during most of the months of the study, except in July and August, when the contribution of accumulation and coarse modes were fairly comparable. The month-to-month variabilities in the complex refractive index (including real $n(\lambda)$ and imaginary $k(\lambda)$ parts) and $\alpha_{440-870}$ were also studied, along with their wavelength dependences. The monthly $n(\lambda)$ varied from 1.46 ± 0.07 in August to 1.58 ± 0.08 in June while $k(\lambda)$ exhibited its maximum at 440 nm in November (0.018 ± 0.010) and its minimum in August (0.003 ± 0.003). In contrast to $k(\lambda)$, the highest monthly $\alpha_{440-870}$ occurred in August, with the value of 0.97 ± 0.02 while its lowest monthly average (0.85 ± 0.04) was found in November. Finally, we investigated an episode involving both urban and dust aerosols as a case study. Aerosol optical properties retrieved from the sun photometer were used to describe the evolution of the aerosol from 2 to 5 November, 2012; Aqua MODIS observations and wind vectors from the NCEP FNL were used to supplement the ground-based measurements in the study.

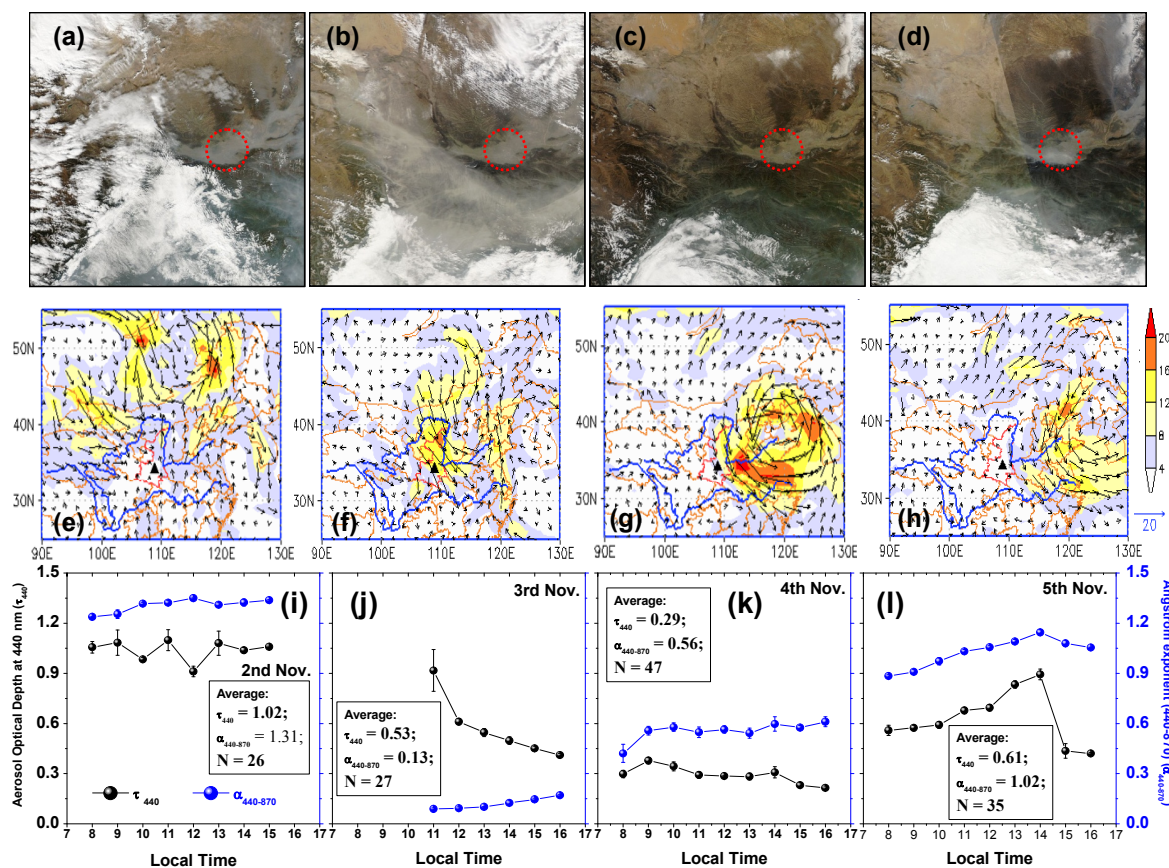


Fig. 7. An episode of aerosol pollution detected by both sun photometer and Aqua MODIS from 2 to 5 November of 2012. MODIS images captured during this period and the associated wind vectors are also presented in (a)–(d) and (e)–(h) with the location of Xi'an city marked with red circles and black triangles, respectively.

The results presented in this paper offer a comprehensive picture of the aerosol in Xi'an, but the spring and winter seasons have not yet been covered. With continuing measurements from the ground-based sun photometer, more opportunities will be provided to perform in-depth studies over this region. These studies will include estimations of aerosol radiative forcing, the evaluation of satellite aerosol retrievals, and participating in the monitoring of pollution caused by particulate matter.

ACKNOWLEDGMENTS

This study was supported by the National Natural Science Foundation of China (41230641, 40925009) and projects from "Strategic Priority Research Program" of the Chinese Academy of Science (Grant No. XDA05100103, XDA05100401, XDB05020401), Ministry of Science & Technology (201209007), and Shaanxi Government (2012KTZB03-01-01).

REFERENCES

Alam, K., Trautmann, T., Blaschke, T. and Majid, H. (2012). Aerosol Optical and Radiative Properties during Summer and Winter Seasons over Lahore and Karachi. *Atmos. Environ.* 50: 234–245.

Bergstrom, R.W., Pilewskie, P., Russell, P.B., Redemann, J., Bond, T.C., Quinn, P.K. and Sierau, B. (2007). Spectral Absorption Properties of Atmospheric Aerosols. *Atmos. Chem. Phys.* 7: 5937–5943.

Cao, J., Wang, Q., Chow, J.C., Watson, J.G., Tie, X., Shen, Z., Wang, P. and An, Z. (2012). Impacts of Aerosol Compositions on Visibility Impairment in Xi'an, China. *Atmos. Environ.* 59: 559–566.

Cao, J.J., Wu, F., Chow, J.C., Lee, S.C., Li, Y., Chen, S.W., An, Z.S., Fung, K.K., Watson, J.G., Zhu, C.S. and Liu, S.X. (2005). Characterization and Source Apportionment of Atmospheric Organic and Elemental Carbon during Fall and Winter of 2003 in Xi'an, China. *Atmos. Chem. Phys.* 5: 3127–3137, doi: 10.5194/acp-5-3127-2005.

Cao, J., Zhang, T., Chow, J.C., Watson, J.G., Wu, F. and Li, H. (2009). Characterization of Atmospheric Ammonia over Xi'an, China. *Aerosol Air Qual. Res.* 9: 277–289.

Cao, Z., Yang, Y., Lu, J., Zhang, C. (2011). Atmospheric Particle Characterization, Distribution, and Deposition in Xi'an, Shaanxi Province, Central China. *Environ. Pollut.* 159: 577–584.

Che, H., Zhang, X., Li, Y., Zhou, Z. and Chen, Z. (2006). Relationship between Horizontal Extinction Coefficient and PM_{10} Concentration in Xi'an, China during 1980–2002. *China Particuology* 4: 327–329.

Che, H., Zhang, X., Alfraro, S., Chatenet, B., Gomes, L.

- and Zhao, J. (2009a). Aerosol Optical Properties and Its Radiative Forcing over Yulin, China in 2001 and 2002. *Adv. Atmos. Sci.* 26: 564–576.
- Che, H.Z., Yang, Z., Zhang, X., Zhu, C., Mac, Q., Zhou, H. and Wang, P. (2009b). Study on the Aerosol Optical Properties and Their Relationship with Aerosol Chemical Compositions over Three Regional Background Stations in China. *Atmos. Environ.* 43: 1093–1099, doi: 10.1016/j.atmosenv.2008.11.010.
- Che, H., Wang, Y. and Sun, J. (2011). Aerosol Optical Properties at Mt. Waliguan Observatory, China. *Atmos. Environ.* 45: 6004–6009.
- Che, H., Wang, Y., Sun, J., Zhang, X., Zhang, X. And Guo, J. (2013). Variation of aerosol optical properties over the Taklimakan Desert in China. *Aerosol Air Qual. Res.* 13: 777–785.
- Chen, J., Jiang, H., Wang, B., Xiao, Z., Jiang, Z., Zhou, G. and Yu, S. (2012). Aerosol Optical Properties from Sun Photometric Measurements in Hangzhou district, China. *Int. J. Remote Sens.* 33: 2451–2461.
- Cheng, T., Wang, H., Xu, Y., Li, H. and Tian, L. (2006a). Climatology of Aerosol Optical Properties in northern China. *Atmos. Environ.* 40: 1495–1509.
- Cheng, T., Liu, Y., Lu, D., Xu, Y. and Li, H. (2006b). Aerosol Properties and Radiative Forcing in Hunshan Dake Desert, Northern China. *Atmos. Environ.* 40: 2169–2179.
- Cong, Z., Kang, S., Smirnov, A. and Holben, B. (2009). Aerosol Optical Properties at Nam Co, a Remote Site in Central Tibetan Plateau. *Atmos. Res.* 92: 42–48.
- de Meij, A., Pozzer, A. and Lelieveld, J. (2012). Trend Analysis in Aerosol Optical Depths and Pollutant Emission Estimates between 2000 and 2009. *Atmos. Environ.* 51: 75–85.
- Dubovik, O. and King, M.D. (2000). A Flexible Inversion Algorithm for Retrieval of Aerosol Optical Properties from Sun and Sky Radiance Measurements. *J. Geophys. Res.* 105: 673–696.
- Dubovik, O., Smirnov, A., Holben, B.N., King, M.D., Kaufman, Y.J., Eck, T.F. and Slutsker, I. (2000). Accuracy Assessments of Aerosol Optical Properties Retrieved from Aerosol Robotic Network (AERONET) Sun and Sky Radiance Measurements. *J. Geophys. Res.* 105: 9791–9806.
- Dubovik, O., Holben, B.N., Eck, T.F., Smirnov, A., Kaufman, Y.J., King, M.D., Tanre, D. and Slutsker, I. (2002). Variability of Absorption and Optical Properties of Key Aerosol Types Observed in Worldwide Locations. *J. Atmos. Sci.* 59: 590–608.
- Dubovik, O., Sinyuk, A., Lapyonok, T., Holben, B. N., Mishchenko, M., Yang, P., Eck, T.F., Volten, H., Munoz, O., Veihelmann, B., van der Zander, W.J., Leon, J.F., Sorokin, M. and Slutsker, I. (2006). Application of Light Scattering by Spheroids for Accounting for Particle Nonsphericity in Remote Sensing of Desert Dust. *J. Geophys. Res.* 111: D11208, doi: 10.1029/2005JD006619.
- Eck, T.F., Holben, B.N., Reid, J.S., Dubovik, O., Smirnov, A., O'Neill, N.T., Slutsker, I. and Kinne, S. (1999). Wavelength Dependence of the Optical Depth of Biomass Burning, Urban and Desert Dust Aerosols. *J. Geophys. Res.* 104: 31333–31350.
- Eck, T.F., Holben, B.N., Dubovik, O., Smirnov, A., Slutsker, I., Lobert, J.M. and Ramanathan, V. (2001). Column-integrated Aerosol Optical Properties over the Maldives during the Northeast Monsoon for 1998–2000. *J. Geophys. Res.* 106: 28: 555–566.
- Eck, T.F., Holben, B.N., Dubovik, O., Smirnov, A., Goloub, P., Chen, H.B., Chatenet, B., Gomes, L., Zhang, X.Y., Tsay, S.C., Ji, Q., Giles, D. and Slutsker, I. (2005). Columnar Aerosol Optical Properties at AERONET Sites in Central Eastern Asia and Aerosol Transport to the Tropical Mid-Pacific. *J. Geophys. Res.* 110: D06202, doi: 10.1029/2004JD005274.
- Fan, X., Chen, H., Xia, X., Li, Z. and Cribb, M. (2010). Aerosol Optical Properties from the Atmospheric Radiation Measurement Mobile Facility at Shouxian, China. *J. Geophys. Res.* 115: D00K33, doi: 10.1029/2010JD014650.
- Fan, X.H., Chen, H.B., Goloub, P., Xia, X.A., Zhang, W.X. and Chatenet, B. (2006). Analysis of Column-integrated Aerosol Optical Thickness in Beijing from AERONET Observations. *China Particuology.* 4:6: 330–335.
- Formenti, P., Schütz, L., Balkanski, Y., Desboeufs, K., Ebert, M., Kandler, K., Petzold, A., Scheuven, D., Weinbruch, S. and Zhang, D. (2011). Recent Progress in Understanding Physical and Chemical Properties of African and Asian Mineral Dust. *Atmos. Chem. Phys.* 11: 8231–8256, doi: 10.5194/acp-11-8231-2011.
- Garland, R.M., Yang, H., Schmid, O., Rose, D., Nowak, A., Achtert, P., Wiedensohler, A., Takegawa, N., Kita, K., Miyazaki, Y., Kondo, Y., Hu, M., Shao, M., Zeng, L.M., Zhang, Y.H., Andreae, M.O. and Pöschl, U. (2008). Aerosol Optical Properties in a Rural Environment near the Mega-city Guangzhou, China: Implications for Regional Air Pollution, Radiative Forcing and Remote Sensing. *Atmos. Chem. Phys.* 8: 5161–5186, doi: 10.5194/acp-8-5161-2008.
- He, Q., Li, C., Geng, F., Yang, H., Li, P., Li, T., Liu, D. and Pei, Z. (2012). Aerosol Optical Properties Retrieved from Sun Photometer Measurements over Shanghai, China. *J. Geophys. Res.* 117: D16204, doi: 10.1029/2011JD017220.
- He, X., Li, C.C., Lau, A.K.H., Deng, Z.Z., Mao, J.T., Wang, M.H. and Liu, X.Y. (2009). An Intensive Study of Aerosol Optical Properties in Beijing Urban Area. *Atmos. Chem. Phys.* 9: 8903–8915, doi: 10.5194/acp-9-8903-2009.
- Holben, B.N., Eck, T.F., Slutsker, I., Tanré, D., Buis, J.P., Setzer, A., Vermote, E., Reagan, J.A., Kaufman, Y.J., Nakajima, T., Lavenu, F., Jankowiak, I. and Smirnov, A. (1998). AERONET - A Federated Instrument Network and Data Archive for Aerosol Characterization. *Remote Sens. Environ.* 66: 1–16.
- Holben, B.N., Tanré, D., Smirnov, A., Eck, T.F., Slutsker, I., Abuhassan, N., Newcomb, W.W., Schafer, J.S., Chatenet, B., Lavenu, F., Kaufman, Y.J., Vande Castle, J., Setzer, A., Markham, B., Clark, D., Frouin, R., Halthore, R., Karneli, A., O'Neill, N.T., Pietras, C., Pinker, R.T., Voss,

- K. and Zibordi, G. (2001). An Emerging Ground-based Aerosol Climatology: Aerosol Optical Depth from AERONET. *J. Geophys. Res.* 106: 12067–12097.
- Jin, M. and Shepherd, J.M. (2005). On Including Urban Landscape in Land Surface Model—How Can Satellite Data Help? *Bull. Am. Meteorol. Soc.* 86: 681–689.
- Kambeidisa, H.D. and Kaskaoutisa, D.G. (2008). Aerosol Climatology over four AERONET Sites: An Overview. *Atmos. Environ.* 42: 1892–1906, doi: 10.1016/j.atmosenv.2007.11.013.
- Kaufman, Y.J., Tanré, D. and Boucher, O. (2002). A Satellite View of Aerosols in the Climate System. *Nature* 419: 215–223.
- Li, C., Mao, J., Lau, K.A., Chen, J.C., Yuan, Z. and Liu, X. (2003). Characteristics of Distribution and Seasonal Variation of Aerosol Optical Depth in Eastern China with MODIS Products. *Chin. Sci. Bull.* 48: 2488–2495.
- Li, Z. (2004). Aerosol and Climate: A Perspective from East Asia, In *Observation, Theory, and Modeling of the Atmospheric Variability*, World Sci., Hackensack, N. J., p. 501–525.
- Li, Z., Xia, X., Cribb, M., Mi, W., Holben, B., Wang, P., Chen, H., Tsay, S.C., Eck, T.F., Zhao, F., Dutton, E.G. and Dickerson, R.R. (2007). Aerosol Optical Properties and Their Radiative Effects in Northern China. *J. Geophys. Res.* 112: D22S01, doi: 10.1029/2006JD007382.
- Li, Z., Blarel, L., Podvin, T., Goloub, P., Buis, J.P. and Morel, J.P. (2008). Transferring the Calibration of Direct Solar Irradiance to Diffuse Sky Radiance Measurements for CIMEL Sun-sky Radiometers. *Appl. Opt.* 47: 1368–1377.
- Li, Z., Goloub, P., Dubovik, O., Blarel, L., Zhang, W., Podvin, T., Sinyuk, A., Sorokin, M., Chen, H., Holben, B., Tanré, D., Canini, M. and Buis, J.P. (2009). Improvements for Ground-based Remote Sensing of Atmospheric Aerosol Properties by Additional Polarimetric Measurements. *J. Quant. Spectrosc. Radiat. Transfer* 110: 1954–1961.
- Li, Z., Li, C., Chen, H., Tsay, S.C., Holben, B., Huang, J., Li, B., Maring, H., Qian, Y., Shi, G., Xia, X., Yin, Y., Zheng, Y. and Zhang, G. (2011). East Asian Studies of Tropospheric Aerosols and their Impact on Regional Climate (EASTAIRC): An Overview. *J. Geophys. Res.* 116: D00K34, doi: 10.1029/2010JD015257.
- Liu, Y., Huang, J., Shi, G., Takamura, T., Khatri, P., Bi, J., Shi, J., Wang, T., Wang, X. and Zhang, B. (2011). Aerosol Optical Properties and Radiative Effect Determined from Sky-radiometer over Loess Plateau of Northwest China. *Atmos. Chem. Phys.* 11: 11455–11463, doi: 10.5194/acp-11-11455-2011.
- Lohmann, U. and Feichter, J. (2005). Global indirect Aerosol Effects: A Review. *Atmos. Chem. Phys.* 5: 715–737, doi: 10.5194/acp-5-715-2005.
- Luo, Y., Lu, D., Zhou, X., Li, W. and He, Q. (2001). Characteristics of the Spatial Distribution and Yearly Variation of Aerosol Optical Depth over China in Last 30 Years. *J. Geophys. Res.* 106: 14501–14514.
- Ma, N., Zhao, C.S., Nowak, A., Müller, T., Pfeifer, S., Cheng, Y.F., Deng, Z.Z., Liu, P.F., Xu, W.Y., Ran, L., Yan, P., Göbel, T., Hallbauer, E., Mildenerger, K., Henning, S., Yu, J., Chen, L.L., Zhou, X.J., Stratmann, F. and Wiedensohler, A. (2011). Aerosol Optical Properties in the North China Plain during HaChi Campaign: An In-situ Optical Closure Study. *Atmos. Chem. Phys.* 11: 5959–5973, doi: 10.5194/acp-11-5959-2011.
- Mahowald, N., Ward, D., Kloster, S., Flanner, M.G., Heald, C.L., Heavens, N., Hess, P., Lamarque, J.F. and Chuang, P. (2011). Aerosol Impacts on Climate and Biogeochemistry. *Annu. Rev. Environ. Resour.* 36: 45–74.
- Pan, L., Che, H., Geng, F., Xia, X., Wang, Y., Zhu, C., Chen, M., Gao, W. and Guo, J. (2010). Aerosol Optical Properties Based on Ground Measurements over the Chinese Yangtze Delta Region. *Atmos. Environ.* 44: 2587–2596, doi: 10.1016/j.atmosenv.2010.04.013.
- Qiu, J.H. and Yan, L.Q. (2000). Variation Characteristics of Atmospheric Optical Depths and Visibility in North China during 1980–1994. *Atmos. Environ.* 34: 603–609.
- Quaas, J., Boucher, O., Bellouin, N. and Kinne, S. (2008). Satellite-based Estimate of the Direct and Indirect Aerosol Climate Forcing. *J. Geophys. Res.* 113: D05204, doi: 10.1029/2007JD008962.
- Roger, J.C., Guinot, B., Cachier, H., Mallet, M., Dubovik, O. and Yu, T. (2009). Aerosol Complexity in Megacities: From Size-resolved Chemical Composition to Optical Properties of the Beijing Atmospheric Particles. *Geophys. Res. Lett.* 36: L18806, doi: 10.1029/2009GL039238.
- Shen, Z., Cao, J., Arimoto, R., Han, Z., Zhang, R., Han, Y., Liu, S., Okuda, T., Nakao, S. and Tanaka, S. (2009). Ionic Composition of TSP and PM_{2.5} during Dust Storms and Air Pollution Episodes at Xi'an, China. *Atmos. Environ.* 43: 2911–2918.
- Shen, Z., Cao, J., Arimoto, R., Han, Y., Zhu, C., Tian, J. and Liu, S. (2010). Chemical Characteristics of Fine Particles (PM₁) from Xi'an, China. *Aerosol Sci. Technol.* 44: 461–472.
- Shen, Z., Cao, J., Liu, S., Zhu, C., Wang, X., Zhang, T., Xu, H. and Hu, T. (2011). Chemical Composition of PM₁₀ and PM_{2.5} Collected at Ground Level and 100 Meters during a Strong Winter-time Pollution Episode in Xi'an, China. *J. Air Waste Manage. Assoc.* 61: 1150–1159.
- Smirnov, A., Holben, B.N., Eck, T.F., Dubovik, O. and Slutsker, I. (2000). Cloud Screening and Quality Control Algorithms for the AERONET Database. *Remote Sens. Environ.* 73: 337–349.
- Smirnov, A., Holben, B.N., Eck, T.F., Slutsker, I., Chatenet, B. and Pinker, R.T. (2002a). Diurnal Variability of Aerosol Optical Depth Observed at AERONET (Aerosol Robotic Network) sites. *Geophys. Res. Lett.* 29: 2115, doi: 10.1029/2002GL016305.
- Smirnov, A., Holben, B.N., Dubovik, O., O'Neill, N.T., Eck, T.F., Westphal, D.L., Guroch, A.K., Pietras, C. and Slutsker, I. (2002b). Atmospheric Aerosol Optical Properties in the Persian Gulf region. *J. Atmos. Sci.* 59: 620–634.
- Smirnov, A., Holben, B.N., Kaufman, Y.M., Dubovik, O., Eck, T.F., Slutsker, I., Pietras, C. and Halthore, R. (2002c). Optical Properties of Atmospheric Aerosol in Maritime Environments. *J. Atmos. Sci.* 59: 501–523.

- Song, L. and Lu, D.R. (2006). Investigation of Atmospheric Optical Characteristics over Shanghai Region. *Clim. Environ. Res.* 11: 203–208 (in Chinese with English Abstract).
- Su, X., Goloub, P., Chiapello, I., Chen, H., Ducos, F. and Li, Z. (2010). Aerosol Variability over East Asia as Seen by POLDER Space-borne Sensors. *J. Geophys. Res.* 115: D24215, doi: 10.1029/2010JD014286.
- Wang, P., Che, H., Zhang, X., Song, Q., Wang, Y., Zhang, Z., Dai, X. and Yu, D. (2010). Aerosol Optical Properties of Regional Background Atmosphere in Northeast China. *Atmos. Environ.* 44:4404–4412.
- Wu, Y., Zhang, R., Pu, Y., Zhang, L., Ho, K.F. and Fu, C. (2012). Aerosol Optical Properties Observed at a Semi-Arid Rural Site in Northeastern China. *Aerosol Air Qual. Res.* 12: 503–514.
- Xia, X., Chen, H. and Wang, P. (2004). Aerosol Properties in a Chinese Semiarid Region. *Atmos. Environ.* 38: 4571–4581.
- Xia, X.A., Li, Z.Q., Holben, B., Wang, P.C., Eck, T., Chen, H.B., Cribb, M. and Zhao, Y.X. (2007a). Aerosol Optical Properties and Radiative effects in the Yangtze Delta Region of China. *J. Geophys. Res.* 112: D22S12, doi: 10.1029/2007JD008859.
- Xia, X., Chen, H., Goloub, P., Zhang, W., Chatenet, B. and Wang, P. (2007b). A Compilation of Aerosol Optical Properties and Calculation of Direct Radiative forcing over an Urban Region in Northern China. *J. Geophys. Res.* 112: D12203, doi: 10.1029/2006JD008119.
- Xie, J. and Xia, X. (2008). Long-term Trend in Aerosol Optical Depth from 1980 to 2001 in North China. *Particuology* 6: 106–111.
- Yan, Q., Hua, D., Wang, Y., Li, S., Gao, F., Zhou, Z., Wang, L., Liu, C. and Zhang, S. (2013). Observations of the Boundary Layer Structure and Aerosol Properties over Xi'an Using an Eye-safe Mie Scattering Lidar. *J. Quant. Spectrosc. Radiat. Transfer* 122: 97–105.
- Yoon, J., von Hoyningen-Huene, W., Vountas, M. and Burrows, J.P. (2011). Analysis of Linear Long-term Trend of Aerosol Optical Thickness Derived from SeaWiFS Using BAER over Europe and South China. *Atmos. Chem. Phys.* 11: 12149–12167, doi: 10.5194/acp-11-12149-2011.
- Yoon, J., von Hoyningen-Huene, W., Kokhanovsky, A.A., Vountas, M. and Burrows, J.P. (2012). Trend Analysis of Aerosol Optical Thickness and Ångström Exponent Derived from the Global AERONET Spectral Observations. *Atmos. Meas. Tech.* 5: 1271–1299, doi: 10.5194/amt-5-1271-2012.
- Yue, D., Hu, M., Wu, Z., Wang, Z., Guo, S., Wehner, B. et al. (2009). Characteristics of Aerosol Size Distributions and New Particle Formation in the Summer in Beijing. *J. Geophys. Res.* 114: D00G12, doi: 10.1029/2008JD010894.
- Zhang, X., Cao, J., Li, L., Arimoto, R., Huebert, B., Wang, D. and Cheng, Y. (2002). Characterization of Atmospheric Aerosol over Xi'an in the South Margin of the Loess Plateau, China. *Atmos. Environ.* 36: 4189–4199.
- Zhao, F. and Li, Z. (2007). Estimation of Aerosol Single Scattering Albedo from Solar Direct Spectral Radiance and Total Broadband Irradiances Measured in China. *J. Geophys. Res.* 112: D22S03, doi: 10.1029/2006JD007384.

Received for review, March 27, 2013
Accepted, September 19, 2013